Dynamic nuclear polarization by two-pulse phase modulation
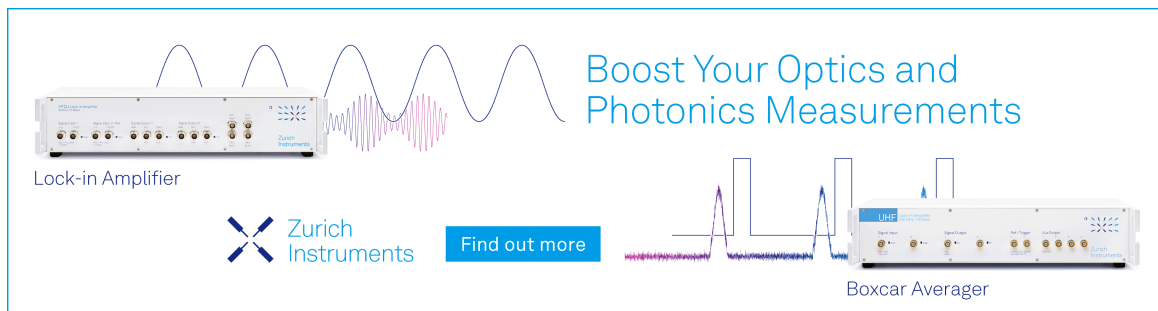
Venkata SubbaRao Redrouthu ⑫ ; Sanjay Vinod-Kumar ⑫ ; Guinevere Mathies ✉ ⑫

Check for updates

View Online   Export Citation

Dynamic nuclear polarization by two-pulse phase modulation

View Online   Export Citation   CrossMark

Venkata SubbaRao Redrouthu, [iD] Sanjay Vinod-Kumar, [iD] and Guinevere Mathies[a) [iD]

AFFILIATIONS

Department of Chemistry, University of Konstanz, Universitätsstrasse 10, 78464 Konstanz, Germany

[a)]Author to whom correspondence should be addressed: guinevere.mathies@uni-konstanz.de

ABSTRACT

The coherent transfer of electron spin polarization to nuclei by means of a microwave pulse sequence is a promising new approach to enhancing the sensitivity of solid-state nuclear magnetic resonance (NMR). The development of pulse sequences for dynamic nuclear polarization (DNP) of bulk nuclei is far from complete, as is the understanding of what makes a good DNP sequence. In this context, we introduce a new sequence, termed Two-Pulse Phase Modulation (TPPM) DNP. We provide a general theoretical description for electron–proton polarization transfer by periodic DNP pulse sequences and find it in excellent agreement with numerical simulations. In experiments at 1.2 T, TPPM DNP generates a higher gain in sensitivity than existing sequences XiX (X-inverse-X) and TOP (Time-Optimized Pulsed) DNP but does so at relatively high nutation frequencies. In contrast, we find that the XiX sequence performs very well at nutation frequencies as low as 7 MHz. A combination of theoretical analysis and experimental investigation makes clear that fast electron–proton polarization transfer, due to a well-preserved dipolar coupling in the effective Hamiltonian, correlates with a short build-up time of the dynamic nuclear polarization of the bulk. Experiments further show that the performances of XiX and TOP DNP are affected differently by the concentration of the polarizing agent. These results constitute important reference points for the development of new and better DNP sequences.

I. INTRODUCTION

Two recent reviews, covering applications in materials science and structural biology, leave no doubt about the added value of combining high-resolution magic-angle spinning (MAS) nuclear magnetic resonance (NMR) with dynamic nuclear polarization (DNP).[1,2] MAS NMR provides detailed information on the local chemical environment of observed nuclei in solids, even if they are amorphous or disordered. DNP adds the extra sensitivity needed to investigate species that inherently occur at low concentrations such as surface sites, intermediates, and (transient) molecular structures embedded in a large protein matrix. DNP has drastically broadened the scope of MAS NMR, and the list of new applications is growing steadily.

Current commercial MAS DNP instrumentation, up to 900 MHz/21.1 T/592 GHz, has been designed around classical DNP mechanisms like the solid-effect[3] and the cross-effect.[4,5] Transfer of electron spin polarization, usually to protons, relies on continuous high-power microwave irradiation at or near the electron Larmor frequency, which is generated by dedicated gyrotrons.[6–8] Output power is tens of watts, which converts into an electron nutation frequency of an MHz or so in the MAS rotor.[9,10] This means that

compared to the other terms in the spin Hamiltonian, the term describing microwave irradiation is weak or of the same order.

An alternate approach to DNP is to transfer electron polarization to nuclei by means of a pulse sequence. With the help of spin dynamics and optimal control, the polarization transfer can be made more efficient, and higher gains in sensitivity can be obtained at reduced average microwave power. During the pulse sequence, however, strong microwave irradiation is needed. Perturbation theories that describe the transfer of polarization by a DNP pulse sequence are only effective when the electron nutation frequency is large (5–10 MHz at least) compared to the electron–nuclear spin interactions. Above 95 GHz, generating high-power microwave pulses with a well-defined frequency and phase is technically challenging, but research is progressing[11,12] and prototypes[13,14] exist. Still, for the time being, pulsed DNP experiments are restricted to low magnetic fields.

Considerable progress has been made in the development of DNP pulse sequences in recent years. In the original DNP pulse sequence NOVEL (Nuclear-spin Orientation Via Electron-spin Locking),[15] a spin lock is applied to the electrons at a nutation frequency that matches the proton Larmor frequency, $|\omega_{1S}| = $

$|\omega_{0I}|$. The sequence is very efficient at low magnetic fields, e.g., at 15 MHz/0.34 T/9.7 GHz (X band),[16,17] but at fields relevant for high-resolution MAS NMR, the NOVEL matching condition demands extremely high microwave power during the lock pulse. This problem was first addressed with the off-resonance NOVEL sequence.[18] By considering the generalized matching condition $\sqrt{\omega_{1S}^2 + \Omega^2} = |\omega_{0I}|$, a low nutation frequency can be compensated by off-resonance irradiation of the electron spins ($\Omega = \omega_{0S} - \omega_{\mu w} \neq 0$). Experiments at 0.34 T showed that NOVEL remains efficient with this relaxed requirement for the electron nutation frequency.

An alternative strategy, which provides further flexibility in the choice of the nutation frequency, was introduced with the TOP (Time-Optimized Pulsed) DNP sequence (Fig. 1).[19] This sequence induces a transfer of polarization when a multiple of the modulation frequency of the sequence ($\omega_m = 2\pi/t_m$) plus or minus the effective frequency (the effective rotation angle of the electron spin magnetization imposed by each block of the sequence, $\omega_{eff} = \beta_{eff}/t_m$) matches the proton Larmor frequency, i.e., $n\omega_{0I} + k\omega_m + l\omega_{eff} = 0$ with $n, l = \pm 1$, $k = \pm 1, \ldots, \pm\infty$. In experiments at 51 MHz/ 1.2 T/34 GHz (Q band), an enhancement factor of 100 was obtained with the TOP DNP sequence at a nutation frequency of 20 MHz. Last year, we introduced the XiX (X-inverse-X) DNP sequence (Fig. 1).[20] The matching condition for XiX DNP has the same form as for TOP DNP, but in experiments at 1.2 T, again at a nutation frequency of 20 MHz, XiX produced a two-times higher gain in sensitivity than TOP DNP. We attributed this to a better preservation of the electron–nuclear dipolar coupling in the effective Hamiltonian, which leads to a faster electron–proton polarization transfer under the influence of the XiX sequence. More recently, an adiabatic implementation of the BEAM (Broadband-Excitation by Amplitude Modulation, see Fig. 1) DNP sequence resulted in an enhancement factor of 360 at 0.34 T.[21] The BEAM sequence follows the same matching condition as TOP and XiX but, nevertheless, a high nutation frequency of 32 MHz (relative to a proton Larmor frequency of 15 MHz) was needed in these experiments. This makes it clear that the suitability of a DNP pulse sequence for enhancing the sensitivity of high-resolution MAS NMR is not determined by the matching condition alone. Instead, it is necessary to investigate the efficiencies of the DNP conditions of a sequence and their dependence on the nutation frequency individually.

Here, we introduce a new member of the TOP/XiX/BEAM family of DNP pulse sequences. The sequence is termed Two-Pulse Phase Modulation (TPPM) DNP (Fig. 1) after the analogous heteronuclear decoupling sequence that is ubiquitously used in MAS NMR.[22] We give a general theoretical description for electron–proton polarization transfer by periodic DNP pulse sequences using operator-based, triple-mode Floquet theory[23,24] and investigate in detail the DNP conditions of the TOP, XiX, and TPPM sequences, including their nutation frequency dependence. In experiments at 1.2 T, the highest gain in sensitivity is obtained with TPPM DNP, but at a relatively high nutation frequency of 33 MHz. Interestingly, XiX DNP performs very well at a nutation frequency of only 7 MHz and hardly improves as the nutation frequency is increased. Experiments also show a correlation between a theoretically predicted fast electron–proton polarization transfer and a short build-up time of dynamic nuclear polarization in bulk. The factor by which the thermal nuclear polarization is finally enhanced, however, is determined by other properties of the sequence. We find,
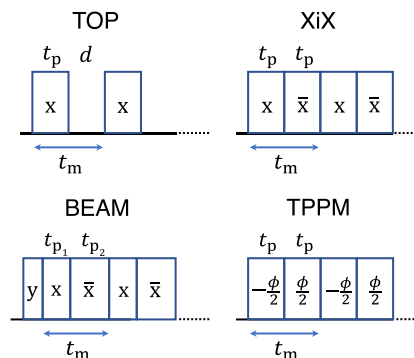

FIG. 1. Family of DNP pulse sequences that follow the matching condition $n\omega_{0I} + k\omega_m + l\omega_{eff} = 0$. The DNP pulse sequences TOP, XiX, and TPPM are investigated at 1.2 T in this work. To build up dynamic nuclear polarization of bulk nuclei (usually protons) in the sample, sequences are repeated thousands of times at a sequence-specific rate.

for example, that the concentration dependence of the enhancement factor is different for XiX and TOP DNP.

II. THEORY AND SIMULATIONS

In this section, we give a (semi-)analytical description of electron–nuclear polarization transfer induced by a periodic microwave pulse sequence and provide specifics on the numerical simulations of this process. The analytical description is an adaptation of the operator-based triple-mode Floquet theory in combination with the Van Vleck–Primas perturbation approach,[25] developed by Scholz *et al.* for de- and recoupling experiments in MAS NMR,[23,24] and specifically the TPPM decoupling sequence.[26] This adaptation was first suggested to describe the TOP DNP sequence[19] and is completed here. We emphasize that we consider for analysis only a single instance of the transfer of electron polarization to a nearby, directly dipolar coupled nuclear spin. Neither the repeated application of the microwave sequence that is required to build up dynamic nuclear polarization of the bulk nor the associated spin diffusion process are included in the modeling. This is an oversimplification, but it is a good starting point, as the efficiency of this initial step plays a crucial role in the pulsed DNP process.

We consider the spin Hamiltonian for a spin system consisting of an electron ($S = 1/2$) interacting with a proton ($I = 1/2$) in a strong magnetic field, in the electron rotating frame and nuclear lab frame, with the appropriate truncations in place. The term for microwave irradiation is tailored to TPPM DNP, but the theoretical description given below is generally applicable to periodic pulse sequences,

$$H(t) = \Omega S_z - \omega_{0I} I_z + \omega_{1S}[\cos(\phi(t))S_x + \sin(\phi(t))S_y] + A S_z I_z + B S_z I_x. \quad (1)$$

In this expression, $\Omega = \omega_{0S} - \omega_{\mu w}$ is the microwave resonance offset frequency, $-\omega_{0I}$ is the nuclear Larmor frequency, ω_{1S} the electron nutation frequency imposed by the microwave irradiation, $\phi(t)$ is a square wave function switching at the modulation frequency $\omega_m = 2\pi/t_m$ between the values $-\phi/2$ and $\phi/2$ (see Fig. 1), A is the secular hyperfine coupling, and B is the pseudo-secular hyperfine

coupling. The pseudo-secular term is due to the electron–proton dipolar coupling and mediates the transfer of polarization.

Under the influence of the microwave pulse sequence, the electron spin magnetization follows a complex trajectory. The periodicity of the sequence is reflected in this trajectory and, hence, it has components at the modulation frequency, ω_m, and its higher harmonics. It also has a component at the effective frequency, $\omega_{eff} = \beta_{eff}/t_m$, where β_{eff} is the effective flip angle of the electron spin magnetization imposed by each repeating unit ("block") of the sequence. $\omega_{eff}(\Omega, \omega_{1S}, t_p, \phi)$ is calculated, for example, with quaternions,[27] and for TPPM DNP, the following analytical expression is found:

$$\omega_{eff} = \cos^{-1}\left\{\cos^2(\omega_a t_p/2) - [\sin^2\theta\cos\phi + \cos^2\theta]\sin^2(\omega_a t_p/2)\right\}/t_p, \quad (2)$$

with $\omega_a = \sqrt{\omega_{1S}^2 + \Omega^2}$ and $\tan\theta = \omega_{1S}/\Omega$.

We apply a series of transformations to a frame in which the size of the Hamiltonian is much reduced and the effects of the electron–proton interactions are conveniently analyzed. We assume that $|\omega_{1S}|, |\omega_{0I}| \gg |A|, |B|$. First, the modulations by the microwave pulse sequence are removed by the time-ordered transformation,

$$U_{1S} = T \exp\left\{-i\int_0^t \Omega S_z + \omega_{1S}[\cos(\phi(t_1))S_x + \sin(\phi(t_1))S_y]dt_1\right\}. \quad (3)$$

We also remove the oscillation at the nuclear Larmor frequency by

$$U_{0I} = e^{i\omega_{0I}I_z t}. \quad (4)$$

In this new, modulating reference frame, the Hamiltonian appears as follows:

$$\begin{aligned}
\tilde{H}(t) &= U_{0I}^{-1}U_{1S}^{-1}H(t)U_{1S}U_{0I} - \Omega S_z \\
&\quad - \omega_{1S}[\cos(\phi(t))S_x + \sin(\phi(t))S_y] + \omega_{0I}I_z \\
&= \tilde{S}_z(t)\left[AI_z + \frac{1}{2}B(I_+e^{-i\omega_{0I}t} + I_-e^{i\omega_{0I}t})\right]. \quad (5)
\end{aligned}$$

The effect of U_{0I} on I_z and I_x is easily found, but the effect of U_{1S}^{-1} on S_z will be analyzed numerically. $\tilde{S}_z(t)$ can, generally, be decomposed into its S_x, S_y, and S_z components, and the time-dependent coefficients can be written as double-mode Fourier series of the two incommensurate frequencies ω_m and ω_{eff}. We, however, still have to do a better job of removing the effects of microwave irradiation. We have to tilt the z-axis such that it aligns with the direction of the effective frequency, $\vec{\omega}_{eff}$,[21,28] which may again be determined with quaternions,

$$U_{tilt} = e^{-\vartheta S_y}e^{-\varphi S_z}, \quad (6)$$

ϑ and φ are the polar and azimuthal angles. In the tilted modulating frame, the time-dependence of the S_z operator simplifies to

$$\begin{aligned}
\tilde{S}_z'(t) &= \frac{1}{2}a_+(t)S_{+'} + \frac{1}{2}a_-(t)S_{-'} + a_z(t)S_{z'} \\
&= \sum_{k=-\infty}^{\infty}\left(\frac{1}{2}a_+^{(k)}e^{i\omega_{eff}t}S_{+'} + \frac{1}{2}a_-^{(k)}e^{-i\omega_{eff}t}S_{-'} + a_z^{(k)}S_{z'}\right)e^{ik\omega_m t}, \quad (7)
\end{aligned}$$

where we have used $S_\pm = S_x \pm iS_y$ and $a_\pm(t) = a_x(t) \mp ia_y(t)$. The primes indicate spin operators in the tilted frame.

Scholz *et al.* have provided the analytical operator-based Floquet description of magnetic resonance experiments that involve three incommensurate frequencies.[23] In TPPM DNP, these are ω_m, ω_{eff}, and ω_{0I}. The time-dependent Hamiltonian in the interaction frame can generally be written as a Fourier series of these three basic frequencies,

$$\tilde{H}(t) = \sum_{n=-\infty}^{\infty}\sum_{k=-\infty}^{\infty}\sum_{l=-\infty}^{\infty}\tilde{H}^{(n,k,l)}e^{in\omega_{0I}t}e^{ik\omega_m t}e^{il\omega_{eff}t}, \quad (8)$$

with $\tilde{H}^{(n,k,l)}$ the Fourier coefficients. At the matching condition,

$$n\omega_{0I} + k\omega_m + l\omega_{eff} = 0, \quad (9)$$

the effective Hamiltonian takes the form

$$\overline{H} = \sum_{n_0,k_0,l_0}\tilde{H}^{(n_0,k_0,l_0)} + \sum_{n_0,k_0,l_0}\tilde{H}_{(2)}^{(n_0,k_0,l_0)} + \cdots. \quad (10)$$

The summation runs over all values of n_0, k_0, l_0 for which the matching condition is fulfilled. The possible values of n, k, l are determined by the terms present in the interaction frame Hamiltonian, i.e., here $n = 0, \pm 1$, $k = 0, \pm 1, \ldots, \pm\infty$, $l = 0, \pm 1$. For TPPM DNP, the terms relevant for polarization transfer arise from the zeroth order and are given by

$$\overline{H}_{DQ} = \frac{1}{4}B\left(a_+^{(k)}S_{+'}I_{+'} + a_-^{(-k)}S_{-'}I_{-'}\right), \quad (11)$$

$$\overline{H}_{ZQ} = \frac{1}{4}B\left(a_+^{(k)}S_{+'}I_{-'} + a_-^{(-k)}S_{-'}I_{+'}\right), \quad (12)$$

depending on whether Eq. (9) is met with opposite [zero quantum (ZQ)] or the same [double quantum (DQ)] or signs of l and n. The state of the spin system is now propagated under this effective Hamiltonian, starting at $\rho(0) = -S_z$. To monitor the transformation of S_z into I_z after contact time t, we use

$$\begin{aligned}
\langle I_z \rangle &= \text{Tr}\{I_z\rho(t)\} \\
&= \text{Tr}\left\{I_z e^{-i\overline{H}t}U_{tilt}^{-1}U_{1S}^{-1}\rho(0)U_{1S}U_{tilt}e^{i\overline{H}t}\right\} \\
&= \langle\rho'(0)|S_{z'}\rangle\text{Tr}\left\{I_z e^{-i\overline{H}t}U_{1S'}^{-1}S_{z'}U_{1S'}e^{i\overline{H}t}\right\} \\
&= \langle\rho'(0)|S_{z'}\rangle\text{Tr}\left\{I_z e^{-i\overline{H}t}S_{z'}e^{i\overline{H}t}\right\}, \quad (13)
\end{aligned}$$

with $\rho'(0) = U_{tilt}^{-1}\rho(0)U_{tilt}$. The last step is only valid under stroboscopic observation, e.g., observation of $\langle I_z \rangle$ only at the end of each applied pulse. Working out the effect of $\overline{H}_{DQ}$ or $\overline{H}_{ZQ}$ on $S_{z'}$ now gives the following simple expressions for the transfer of longitudinal magnetization:

$$\langle I_z \rangle_{DQ}(t) = \frac{1}{2}\langle\rho'(0)|S_{z'}\rangle\left[\cos\left(\frac{1}{2}B\sqrt{a_+^{(k)}a_-^{(-k)}}t\right) - 1\right], \quad (14)$$

$$\langle I_z \rangle_{ZQ}(t) = \frac{1}{2}\langle\rho'(0)|S_{z'}\rangle\left[1 - \cos\left(\frac{1}{2}B\sqrt{a_+^{(k)}a_-^{(-k)}}t\right)\right]. \quad (15)$$

The rate of the polarization transfer is determined by the strength of the dipolar coupling (specifically the size of the pseudo-secular

term, B) together with the scaling factor, $\kappa = \sqrt{a_+^{(k)} a_-^{(-k)}}$. The amplitude of the oscillation is determined by the alignment,[29] $\langle \rho'(0) | S_{z'} \rangle$, which is the scalar projection of $\rho'(0)$ on $S_{z'}$ (the direction of $\vec{\omega}_{eff}$). The alignment determines how much magnetization can eventually be transferred. An unfavorable alignment can be improved with a preparation pulse, which creates the desirable $\rho(0)$, as is performed in NOVEL and BEAM.[15,21] After powder averaging, an alignment of one will lead to a final $\langle I_z \rangle$ of ± 0.5.

The basic spin system for numerical simulations consists of an electron and a proton 3.5 Å apart, corresponding to a dipolar coupling of 1.8 MHz. The strength of the coupling was adjusted to reproduce the dependence of the enhanced ^{1}H NMR signal on the contact time ("contact curves") in (off-resonance) NOVEL experiments with trityl OX063 in DNP juice at 0.34 T[17,18] and is considerably stronger than the individual electron–proton couplings observed in electron paramagnetic resonance (EPR) experiments on Finland trityl.[30,31] The reason is that the unpaired electron of trityl OX063 is surrounded by tens of protons at similar distances, which are simultaneously available for polarization transfer. Analogous to the intensity of the spin–flip lines in the EPR spectrum of trityl, this can be modeled by an increased effective dipolar coupling.[31–33]

The numerical simulations were built around the kernel of the magnetic resonance simulation library Spinach.[34] Starting in thermal equilibrium, the density matrix is propagated numerically. After the DNP pulse sequence has been applied for the duration of the contact time t, the z-magnetization of the proton spins is again read out by $\langle I_z \rangle(t) = \text{Tr}\{I_z \rho(t)\}$. As protons have spin $I = 1/2$, $\langle I_z \rangle$ equals half the normalized population difference, i.e., half the proton spin polarization. To enable comparison to the results of the semi-analytical analysis described earlier, in which $\rho(0) = -S_z$, the proton spins are initially saturated and the high-field and high-temperature limits are assumed,

$$\rho(0) \approx \text{Id} - \frac{\hbar \omega_{0S}}{k_B T} S_z. \tag{16}$$

Semi-analytically and numerically calculated contact curves are compared after powder averaging.

To predict where the best pulsed DNP conditions will occur in the experiment, g-anisotropy ($g_x = g_y = 2.003\,19$, $g_z = 2.002\,58$) and a second proton, located at 3.5 Å from the electron and at 2.7 Å from the first proton, are included in the numerical simulations. In this case, $\langle I_z \rangle$ with $I_z = I_{z,1} + I_{z,2}$ (summing over the two ^{1}H spins) is calculated. To translate this to the enhancement factor ε_B (see Sec. III), $\langle I_z \rangle(t)$ is divided by $\langle I_{z,1} \rangle(0)$, which is the proton z-magnetization at thermal equilibrium (note that in our spin system, the two protons are equivalent). Simulations were run in Hilbert space, and relaxation was not included unless noted otherwise. Typical two-dimensional parameter scans run readily on a workstation. However, extended sets of simulations of TOP/XiX/TPPM DNP were performed on the Scientific Compute Cluster (SCC) of the University of Konstanz.

III. EXPERIMENTAL METHODS

Pulsed DNP experiments were performed at 34 GHz/1.2 T/ 51 MHz on a Bruker Elexsys E580 pulsed EPR spectrometer with Q-band extension (SuperQ-FT-u bridge). The pulse programmer was a PatternJet II with a 2 ns resolution. Pulses were amplified with a prototype BLA50 ESR 33–35 GHz 50 W amplifier (Bruker BioSpin GmbH). The microwave power is attenuated after amplification and only a maximum of about 20 W reaches the resonator. This typically generates a maximum electron nutation frequency of 40 MHz in the microwave resonator of the EN 5107D2 EPR/ENDOR probe when it is fully overcoupled. A few experiments reported herein were performed with an HA8019 33–35 GHz 10 W amplifier (HBH Microwave GmbH). With this amplifier, the maximum power at the resonator is about 4 W, and the maximum nutation frequency is about 19 MHz. Each second pulse in TPPM DNP was generated with an MPFU (microwave pulse forming unit), whose relative phase was calibrated against the x-channel of the spectrometer.

The EPR/ENDOR probe was made suitable for ^{1}H NMR at 51.7 MHz with a detachable tuning/matching box. NMR experiments were controlled by an iSpin-NMR console (SpinCore Technologies, Inc.), and RF pulses were amplified using a refurbished LPI-10 amplifier (E & I). The ^{1}H NMR signal was detected with a Hahn echo, $(t_{90})_x - \tau - (t_{180})_x - \tau-$, with $t_{90} = 3.5\ \mu s$ and the EXORCYCLE phase cycle.[35] For quantitative comparisons, τ was set to 40 μs, as this suppresses the proton background signal from the probe relative to the proton signal from the sample. A recycle delay of 44 s was used for these measurements. All other experiments were performed with a τ of 20 μs and a recycle delay of 24 s.

Samples consisted of a frozen glassy matrix of d_8-glycerol:D_2O:H_2O 60:30:10 v:v:v (a.k.a. "DNP juice") doped with trityl OX063 (Polarize ApS).[17] Echo-detected EPR spectra are shown in Fig. S1. Quartz sample tubes had an outer diameter of 1.6 mm and were fused on one end. The sample volume was 1–2 μl. During the experiments, the sample temperature was kept at 80 K using a CF 935 flow cryostat (Oxford Instruments) and He as a cryogen. The concentration of trityl OX063 was verified for all samples by UV/Vis absorption at 266 nm (molar absorption coefficient 35 000 $M^{-1}\ cm^{-1}$)[36] using a Cary 60 spectrophotometer (Agilent Technologies).

Enhancement factors of the ^{1}H spin polarization relative to thermal equilibrium are calculated according to

$$\varepsilon_B = \frac{I_{on}}{I_{off}} \cdot \frac{\left(1 - e^{-rd_{off}/T_{1n}}\right)}{\left(1 - e^{-rd_{on}/T_{BU}}\right)}. \tag{17}$$

In this expression, I_{on} and I_{off} are the intensities of the ^{1}H NMR signals measured with microwaves on and off, rd_{on} and rd_{off} are the recycle delays used in both experiments, T_{BU} is the build-up time of the bulk proton polarization, and T_{1n} is the proton spin-lattice relaxation time.[37] Considering that averaging of an NMR signal is typically required, that the signal-to-noise ratio increases with the square root of the number of averages, and that the recycle delay in a DNP/NMR experiment is restricted by T_{BU}, the practical sensitivity gain for a fixed total experiment time is given by $|\varepsilon_B| \sqrt{T_{1n}/T_{BU}}$.[38] The probe gives rise to a background signal, which was measured separately and subtracted from the ^{1}H NMR signals observed when the sample was present before I_{on}/I_{off} was determined. Quantitative comparisons of ^{1}H NMR signal intensities were only made within a single measurement session during which the cooling was not interrupted and the sample was not removed from the cryostat.

IV. RESULTS

The experimentally relevant parameter space of TPPM DNP at 1.2 T was explored in full by means of numerical simulations. ε_B was evaluated after a contact time of 800 ns in two-dimensional parameter scans in which the microwave resonance offset was varied from -110 to 110 MHz and the nutation frequency from 0 to 40 MHz. These parameter scans were performed for pulse lengths of $4, 6, 8, \ldots, 82$ ns and phase differences between the pulses of $5°, 10°, 15°, \ldots, 180°$. Conditions of interest, i.e., a particularly high $|\varepsilon_B|$, are shown together in Fig. S2. Of the experimentally investigated conditions, the combination of $t_p = 16$ ns and $\phi = 120°$, see the simulation in Fig. 2, was found to produce the highest enhancement factor.

Experimental investigation of conditions of interest involved an iterative process in which the nutation frequency, resonance offset, phase, and repetition time of the pulse sequence were subsequently and repeatedly optimized to produce the highest ^{1}H NMR intensity. For the 16 ns/120° condition, the results of the optimizations of the resonance offset and the phase are shown in Fig. 3, for a nutation frequency of 33 MHz. Upon optimization, this condition close to resonance (2–4 MHz) fared better than the condition further off resonance (15–25 MHz) at a nutation frequency of 38 MHz (see Fig. 2). The optimal phase difference was found to be 115°, not 120°, but this may be due to uncertainty in the phase calibration. The 16 ns/120°
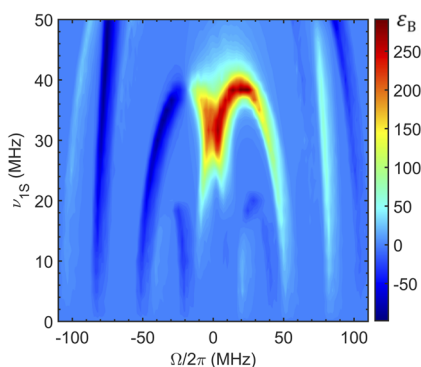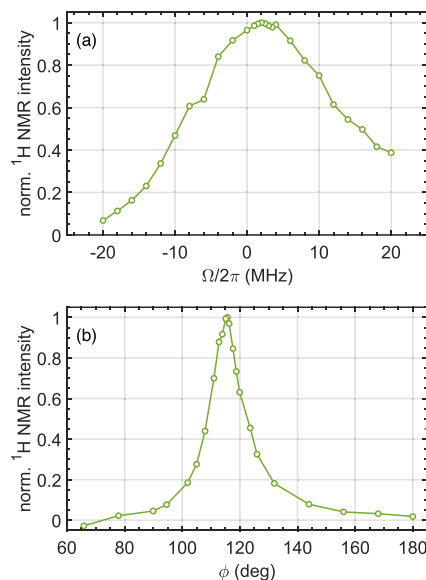

FIG. 3. (a) Experimental field profile and (b) phase optimization of TPPM DNP around the condition $t_p = 16$ ns, $\phi = 120°$, and $\nu_{1S} = 33$ MHz. The trityl concentration was 6.4 mM.

FIG. 2. Parameter scan (simulation) of TPPM DNP with $t_p = 16$ ns and $\phi = 120°$ at 1.2 T (^{1}H Larmor frequency of 51.7 MHz). The contact time is 20 μs. After this long time, oscillations in ε_B, due to well-defined dipolar couplings, are largely averaged out (see Fig. S3 for an illustration).
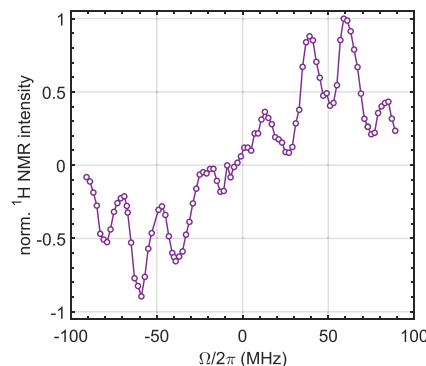

FIG. 4. Experimental field profile of XiX DNP at 18 MHz. Note that for XiX and also for TOP, the best DNP conditions are always found off-resonance. The trityl concentration was 5.7 mM. A detailed investigation of the central region of this field profile (close to resonance) is included in the supplementary material, Figs. S7 and S8.

TABLE I. Parameters and results of pulsed DNP experiments performed on a sample with a trityl concentration of 6.4 mM. The ^{1}H longitudinal relaxation time was found to be 52 s (Fig. S5). For TOP with high nutation frequency, XiX, and TPPM, a contact time of ~1 μs is sufficient to complete the polarization transfer [Fig. 8(b)]. Hence, for these sequences, the average microwave powers can be further reduced to 82, 16, 21, and 12 mW, respectively, without adversely affecting the enhancement factors.

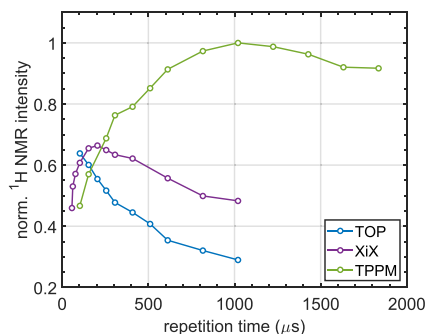|	t_p, d (ns), ϕ	$\frac{\Omega}{2\pi}$ (MHz)	κ	$\langle \rho'_0 | S_{z'} \rangle$	ν_{1S} (MHz)	t_c (ns)	Rep. time (μs)	Avg. power (mW)	$\frac{I_{on}}{I_{off}}$	T_{BU} (s)	ε_B	$|\varepsilon_B|\sqrt{\frac{T_{1n}}{T_{BU}}}$
TOP	10, 14	95	0.10	-1.00	19	7200	102	93	201	26	141	199
TOP	10, 14	92	0.21	-1.00	40	7200	102	590	218	20	140	226
XiX	48, 180°	-39	0.21	1.00	19	3456	204	54	-193	19	-123	203
XiX	48, 180°	-60	0.21	1.00	19	3456	153	72	-227	19	-144	238
TPPM	16, 115°	2	0.34	0.98	33	9600	1020	120	281	15	170	316

FIG. 5. Optimization of the repetition times for TOP (ν_{1S} = 19 MHz), XiX ($\Omega/2\pi = -39$ MHz), and TPPM DNP ($\phi = 120°$) at the conditions shown in Table I. For XiX, the absolute value of the normalized ^{1}H NMR intensity is plotted for clarity. The trityl concentration was 6.4 mM.

condition, after optimization, was better than the 14 ns/80° and 18 ns/155° conditions, even though the simulations suggest these are of similar or better quality (Fig. S2).

In a series of experiments on a sample containing 6.4 mM trityl [Fig. S1(a)], the gain in sensitivity obtained with TPPM DNP at the 16 ns/120° condition was compared to the gains in sensitivity obtained with XiX and TOP DNP. For the latter two sequences,

the conditions were chosen as previously published: the nutation frequency was 18–19 MHz; for XiX,[20] t_p = 48 ns; and for TOP,[19] t_p = 10 ns, d = 14 ns. The experimental field profile of XiX DNP was remeasured and shown in Fig. 4. Contrary to our earlier observation at 2.5 mM,[20] the $\Omega/2\pi = \pm60$ MHz conditions produce higher enhancement factors than the $\Omega/2\pi = \pm39$ MHz conditions. The optimized microwave-on signals of TOP, XiX, and TPPM DNP are shown together in Fig. S4. The spin-lattice relaxation time of the proton spins was also measured (Fig. S5), as were the bulk build-up times, T_{BU}, at each condition (Fig. S6). Enhancement factors, ε_B, can now be determined following Eq. (17) and are shown in Table I. Compared to XiX and TOP, TPPM DNP produces a 20% higher enhancement of proton polarization. The short T_{BU} of TPPM DNP (15 s) makes this improvement more pronounced when the practical sensitivity gain, $|\varepsilon_B|\sqrt{T_{1n}/T_{BU}}$, is considered (see Table I).

Figure 5 shows $|I_{on}|$ as a function of the repetition time of the TOP, XiX, and TPPM sequences. The optimal repetition time is considerably longer for TPPM (1020 μs) than for XiX and TOP DNP (102 and 204 μs). As a consequence, even though the nutation frequency required for the TPPM sequence to induce an $e^- - {}^1$H polarization transfer is higher than for XiX and TOP DNP, the average applied microwave power is comparable (120 vs 72 and 93 mW). Interestingly, for TPPM DNP, choosing a repetition time shorter than 1020 μs reduces the build-up time of the bulk polarization (see Fig. S9). The decrease in $|I_{on}|$ is, however, not fully compensated, and the practical sensitivity gain is still reduced.
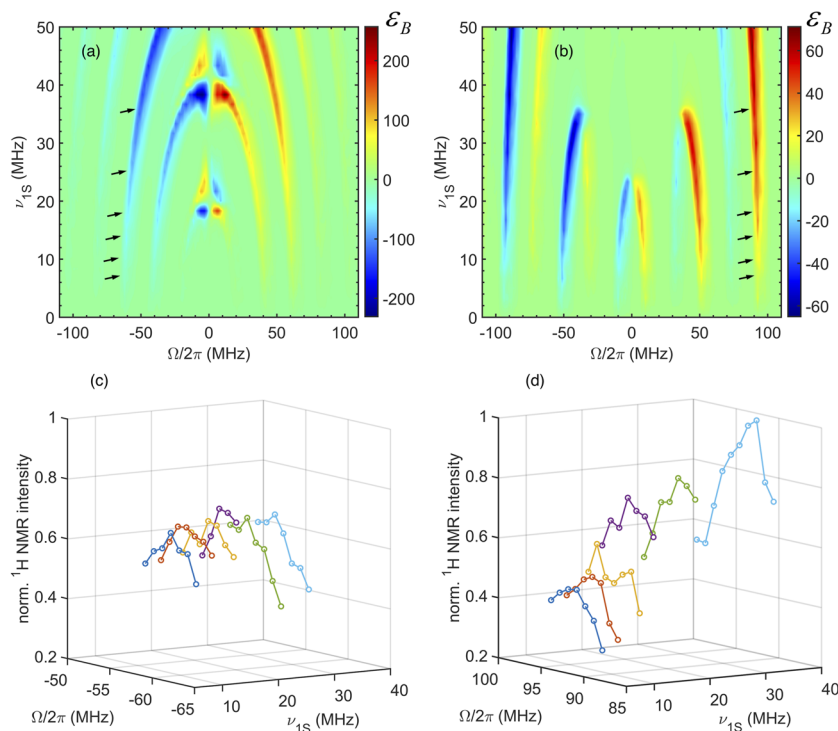

FIG. 6. (a) and (b) Parameter scans (simulations) of XiX DNP, with t_p = 48 ns, and TOP DNP, with t_p = 10 ns and d = 14 ns. The contact time is 20 μs. (c) and (d) Experimental investigation of the nutation frequency dependence of XiX and TOP DNP. Both figures show optimizations of the resonance offsets at the nutation frequencies indicated by arrows in (a) and (b). Supporting data for these figures can be found in Table S1.

04 April 2024 14:49:11

Parameter scans of XiX and TOP DNP show nearly vertical, narrow regions of positive and negative enhancements, which come together at high nutation frequencies [see the simulations in Figs. 6(a) and 6(b)]. This makes it possible to experimentally investigate the nutation frequency dependence of the DNP efficiency for these sequences in a straightforward manner, i.e., without changing other parameters. Enhanced ^{1}H NMR signals were measured at the conditions indicated by the arrows, following the $\Omega/2\pi = -60$ MHz condition of XiX and the $\Omega/2\pi = +95$ MHz condition of TOP. At each nutation frequency, the microwave resonance offset was optimized, and the resulting mini-field profiles are plotted in Figs. 6(c) and 6(d). Repetition times were optimized at each nutation frequency, and bulk build-up times were measured (see Table S1). In the case of XiX, the intensity of the enhanced ^{1}H NMR signal barely changes, while in the case of TOP, the intensity increases significantly with the nutation frequency. Table S1 makes clear that this increase is mostly due to a decrease in T_{BU}, from 65 to 29 s, at a constant optimal repetition time. For XiX, the decrease in T_{BU} is much less pronounced, from 29 down to 20 s, but the optimal repetition time is lengthened.

Figures 7(a)–7(c) show representative trajectories of S_z in the modulating interaction frame for TOP, XiX, and TPPM DNP. The scaling factors are calculated by double-mode Fourier analysis of these trajectories (see Sec. II) and are listed in Table I, along with the alignments. Corresponding semi-analytical contact curves [solid lines, Eqs. (14) and (15), followed by powder averaging] are plotted in Fig. 7(d). The initial rise of $\langle I_z \rangle(t)$ and the time of the first maximum are determined by the strength of the $e^- - {}^1$H dipolar coupling times the scaling factor. Therefore, the curves show the faster transfer of polarization induced by the TPPM sequence ($\kappa = 0.34$) compared to XiX ($\kappa = 0.21$) and TOP ($\kappa = 0.10$). After this, the curves oscillate around $\langle I_z \rangle = 0.5$ (corresponding to an enhancement factor ε_B of 329), as expected after powder averaging and for alignments very close to 1 (Table I). The agreement with numerical propagation [dashed lines in Fig. 7(d)] is excellent, showing that the perturbation theory approach works well.

A comparison of the TOP, XiX, and TPPM sequences at different conditions in Table I shows that a larger scaling factor leads to a shorter T_{BU}. The investigation of the nutation dependence essentially shows the same (see Table S1). For both XiX and TOP DNP, the scaling factor increases with the nutation frequency, with the scaling factor of the former being approximately twice as large. For both sequences, this leads to a reduction of T_{BU}, which is, as noted earlier, more drastic for TOP than for XiX. In the case of XiX, the increase in the optimal repetition time likely mitigates the positive effect of the larger scaling factor.

Numerically simulated contact curves, which take into account g-anisotropy, a second proton, as well as electron and nuclear spin
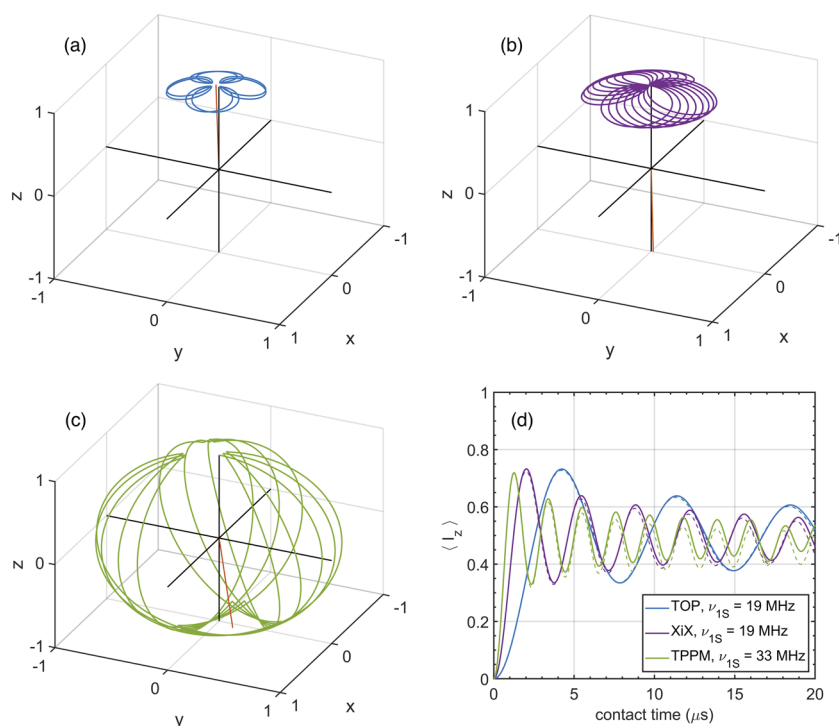

FIG. 7. (a)–(c) Trajectories of S_z in the modulating interaction frame for TOP ($t_p = 10$ ns, $d = 14$ ns, $\nu_{1S} = 17.8$ MHz, $\Omega/2\pi = 92.61$ MHz), XiX ($t_p = 48$ ns, $\nu_{1S} = 17.8$ MHz, $\Omega/2\pi = 59.49$ MHz), and TPPM DNP ($t_p = 16$ ns, $\phi = 120°$, $\nu_{1S} = 33.0$ MHz, $\Omega/2\pi = 5.49$ MHz). Eight blocks of each sequence are applied. The direction of the effective frequency is indicated by the red lines. (d) Solid lines: semi-analytical contact curves, after powder averaging of Eqs. (14) and (15). Scaling factors and alignments are calculated as described in Sec. II. Dashed lines: contact curves calculated by numerical propagation of the density matrix after powder averaging. An electron dipolar coupled to a single proton was considered; no g-anisotropy was taken into account.

relaxation, are shown for TOP, XiX, and TPPM DNP in Fig. 8(a). The fast initial increase of ε_B is again determined by the scaling factor, with TPPM being faster than XiX and XiX being faster than TOP. The oscillations are less pronounced than in Fig. 7(d) and fade at longer contact times. Due to relaxation, for TPPM DNP, the enhancement factor decays with the contact time, whereas for XiX, it remains roughly constant, and for TOP, it even goes up slightly. This can be qualitatively understood from the modulating frame trajectories in Figs. 7(a)–7(c). These trajectories show $U_{1S}^{-1} S_z U_{1S}$ [U_{1S} is defined in Eq. (3)] but also offer a visualization of the evolution of the electron spin magnetization in the electron rotating frame under the influence of the microwave pulse sequences [$U_{1S}(-S_z)U_{1S}^{-1}$]. For TOP and XiX, the magnetization vector stays close to the z-axis, meaning that the contributions of S_x and S_y are small at all times. For TPPM, however, the magnetization traverses the entire unit sphere, and the contributions of S_x and S_y are large. This makes TPPM, more than XiX and TOP, susceptible to (fast) transverse relaxation.

Figure 8(a) reveals another characteristic of the TPPM DNP sequence. Compared to Fig. 7(d), the final enhancements, i.e., at long contact times, are reduced for all three sequences, but particularly severely for XiX (ε_B is about 80 at 20 μs) and TOP (ε_Bs are about 60 and 80 at 20 μs). This reduction is mostly due to line-broadening caused by the g-anisotropy of trityl, to which TPPM is much less sensitive than the other two sequences. The reason is apparent when
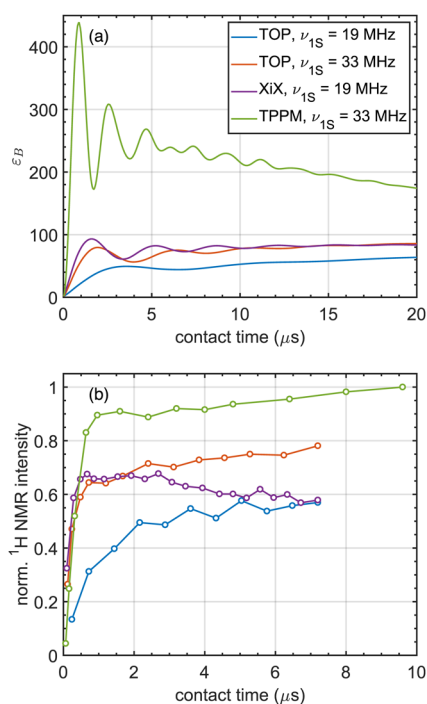
the effective frequency is plotted as a function of the resonance offset for the 16 ns/120° TPPM DNP condition (see Fig. S10). The matching condition [Eq. (9)] is met for $k = 2$ and $l = -1$, and the curve $2\nu_{1S} - \nu_{\text{eff}}$ sheers along the ^{1}H Larmor frequency, meaning that the mismatch is small across a large offset range. A similar phenomenon has been observed for the BEAM sequence at 0.34 T.[21]

Contact curves were also experimentally investigated, and the results are plotted in Fig. 8(b). For TPPM, XiX, and high-nutation TOP, the characteristic fast rise and plateau are observed.[18] For XiX and high-nutation TOP, the rise times are considerably faster than expected from the scaling factor and numerical simulations. For TPPM, the expected decay of the enhancement at longer contact times due to transverse relaxation is not observed. The XiX contact curve, however, does decay slightly. For low-nutation TOP, the shape of the contact curve has become exponential. Together with the quantitative experiments summarized in Table I, Figs. 8(a) and 8(b) suggest that the simulations overestimate the performance of TPPM but underestimate it for XiX and TOP.

When we first introduced the XiX DNP sequence,[20] we reported a maximum enhancement factor of 58 and a $|\varepsilon_B|/\sqrt{T_{\text{BU}}}$ of 12. For TOP DNP, in the same series of experiments, we obtained a maximum enhancement factor of 40 and a $|\varepsilon_B|/\sqrt{T_{\text{BU}}}$ of 6. Thus, in these experiments, XiX fared much better than TOP, while in the current set of experiments, the difference in performance between XiX and TOP is not as pronounced (Table I). The earlier experiments were performed on a sample containing 2.5 mM trityl and at a nutation frequency of about 18 MHz, which was generated by operating a 10 W amplifier at full power. The results reported in Table I were obtained from a sample containing 6.4 mM trityl and with a 50 W amplifier, whose output power was attenuated. All other experimental conditions were the same as before. To investigate this discrepancy, we performed a new series of pulsed DNP experiments with a sample containing 2.1 mM trityl [Fig. S1(b)]. ^{1}H NMR spectra enhanced by XiX and TOP DNP induced with the 10 W or the 50 W amplifier are plotted together in Fig. S11. These experiments reproduce the high gain in sensitivity achieved by XiX DNP relative to TOP, as we observed previously, and show that the choice of the amplifier has only a minor effect. Hence, we conclude that the change in relative performance cannot be attributed to subtle differences in the microwave irradiation by the different amplifiers but instead arises from the difference in the polarizing agent concentrations.

FIG. 8. Numerically simulated contact curves for TOP, XiX, and TPPM DNP at resonance offsets of 92, 61, and 3 MHz. An electron dipolar coupled to two ^{1}Hs was considered; g-anisotropy was taken into account, as was relaxation with the following parameters: $T_{1e} = 1$ ms, $T_{2e} = 5$ μs, $T_{1n} = 13$ s, and $T_{2n} = 1$ ms. (b) Corresponding experimental contact curves for TOP, XiX, and TPPM. The repetition times were 102 (153 at 33 MHz nutation), 153, and 816 μs, respectively. The recycle delay was 24 s. The trityl concentration was 5.7 mM.

V. DISCUSSION

We have investigated the conditions under which the TPPM sequence generates DNP both with numerical simulations and experimentally at 34 GHz/1.2 T/51 MHz. For a pulse length t_P of 16 ns, a phase difference ϕ of 120°, and a nutation frequency ν_{1S} of 33 MHz, the TPPM sequence provides a practical sensitivity gain of $|\varepsilon_B|\sqrt{T_{1n}/T_{\text{BU}}} = 316$ in a sample of 6.4 mM trityl OX063 in DNP juice. This is more than could be obtained with XiX ($|\varepsilon_B|\sqrt{T_{1n}/T_{\text{BU}}} = 238$) or TOP DNP ($|\varepsilon_B|\sqrt{T_{1n}/T_{\text{BU}}} = 226$) under the same conditions. We attribute the good performance of the TPPM sequence to a high offset tolerance (insensitivity to line-broadening by g-anisotropy) and a large scaling factor, which leads to a fast build-up of the bulk nuclear polarization.

The four DNP pulse sequences TOP, XiX, TPPM, and BEAM all follow the flexible, high-field compatible matching condition of Eq. (9). However, that matching can be accomplished does not guarantee that polarization transfer is efficient or that high enhancement factors can be obtained. This is determined by the pulse (and delay) lengths, the phases of the pulses, the nutation frequency, and the microwave resonance offset in a different way for each sequence. An important point to keep in mind is that maintaining the DNP efficiency requires linear scaling of the pulse (and delay) lengths, the nutation frequency, and the resonance offset with the magnetic field. Thus, when appropriately scaled, the simulated parameter scans in Figs. 2, 6, and S2 also give a good indication of the efficiency of TOP, XiX, and TPPM at higher magnetic fields. This means that the good performance of TPPM DNP at 1.2 T, which required a high nutation frequency of 33 MHz (relative to 51 MHz), will be difficult to reproduce at magnetic fields suitable for high-resolution MAS NMR, even though, due to the long optimal repetition time, a high average microwave power is not needed (see Table I). On the other hand, this makes the efficiency of XiX DNP at a nutation frequency of 7 MHz, which was not predicted by our simple modeling (see below), all the more interesting.

By means of the operator-based, triple mode Floquet theory, we could derive the DQ and ZQ effective Hamiltonians of Eqs. (11) and (12). They determine the evolution of the state of the spin system under the influence of the DNP pulse sequence at the matching condition [Eq. (9)]. The analytical expression for the time-dependence of the longitudinal magnetization of the nuclear spins, $\langle I_z \rangle (t)$ [Eqs. (14) and (15)], has just two parameters: the scaling factor, $\kappa = \sqrt{a_+^{(k)} a_-^{(-k)}}$, and the alignment, $\langle \rho'(0) | S_{z'} \rangle$. Once these parameters are determined, contact curves are in excellent agreement with numerical simulations [Fig. 7(d)]. Wili et al.[21] derived the effective Hamiltonian by means of average Hamiltonian theory. To be able to obtain a time-independent effective Hamiltonian by averaging, they performed an additional frame transformation that removes the oscillation at the effective frequency. The agreement with numerical simulations in this case is also excellent. The advantage of their approach is that polarization transfer is also described when the matching condition is not perfectly met. This is cumbersome with Floquet theory. However, a strategy to deal with this issue has recently been devised.[39]

The plots of $\tilde{S}_z(t)$ in the modulating frame in Figs. 7(a)–7(c) help to gain intuitive insight into the TOP, XiX, and TPPM DNP sequences. For example, from these trajectories, it is immediately clear why neither TOP nor XiX nor TPPM (with $t_p = 16$ ns and $\phi = 120°$) benefit from a preparation pulse. In all three cases, $\bar{\omega}_{eff}$ is pretty much along the z-axis, and the alignment is close to ±1. In the case of TPPM, which works best close to resonance, the gradual precession at ω_{eff} (approximately) around the z-axis is made possible by the phase difference, ϕ, between the pulses. The case of high-nutation frequency BEAM at 0.34 T (X band),[21] which works best with a 90° preparation pulse along y, is visualized in Fig. S12. The pulses of unequal lengths, applied close to resonance and alternating between x and −x, cause a precession around (approximately) the −x-axis. The preparation pulse is thus mandatory to obtain good alignment. Since the z-axis and $\bar{\omega}_{eff}$ approximately align, the trajectories in Figs. 7(a)–7(c) also visualize the large scaling factor of XiX compared to TOP DNP and the still larger scaling factor of

TPPM. As $\tilde{S}_z(t)$ moves further away from the z-axis, the x- and y-components of $\tilde{S}_z(t)$ are accordingly larger.

The extensive set of experimental data at 1.2 T provides new, practical insight into pulsed DNP. An important observation is that a larger scaling factor leads to a faster build-up time of the bulk polarization, T_{BU} (Tables I and S1). A shorter repetition time also leads to a shorter T_{BU} (Fig. S9) and, in addition, to a higher $|\varepsilon_B|$ (Fig. 5); however, for XiX and TPPM, only down to an optimum value (see below). These behaviors resemble those of the classical solid-effect, where a higher applied microwave power leads to a shorter T_{BU} and a higher enhancement factor.[40] In line with intuition, the more vigorously the electron polarization is pumped into the nuclear spin bath, the higher the maximum enhancement factor and the faster it is reached. More vigorous pumping can be accomplished by applying small strokes as often as possible, i.e., by continuous microwave irradiation, or by applying highly efficient strokes at a slower, optimized pace, i.e., by a well-chosen and well-timed microwave pulse sequence.

While TPPM provides a higher gain in sensitivity than XiX and TOP, the improvement is not as large as expected from the simulations [Fig. 8(a)]. This is likely related to the long optimal repetition rate of TPPM DNP (Fig. 5). Before another effective transfer of polarization can take place, the electron spin magnetization must have returned to thermal equilibrium, i.e., to −z. This means that the pace at which a DNP pulse sequence is best repeated depends on the longitudinal relaxation rate of the electron spins and the final direction of the magnetization at the end of the contact time. With this in mind, the trajectory in Fig. 7(c) offers no obvious explanation for the long optimal repetition time of TPPM DNP. At the end of each block, the magnetization is brought back close to where it started. Possibly, after many cycles of transfer, due to EPR line width, pulse imperfections, and an inhomogeneous B_1-field, the magnetization fans out. When the TPPM sequence is applied again, many spin packets no longer follow the ideal trajectory shown in Fig. 7(c). They may end up close to the x, y-plane, from where it takes a long time to get back to −z. A potential solution to this problem would be to design a TPPM sequence consisting of composite pulses[41] or make use of phase or super cycles,[42] taking care to keep all spin packets together even after many cycles of transfer.

The rise time in the contact curves in Figs. 8(a) and 8(b) is well predicted by the simulations for TPPM, but for XiX and TOP, the prediction is too slow. The rise time depends on the scaling factor and on the effective electron–proton dipolar coupling. As described in Sec. II, the value of the dipolar coupling used in the simulations has been adjusted empirically to reproduce the rise time in experimental contact curves of (off-resonance) NOVEL with trityl OX063 in DNP juice at the X band.[17,18] If we assume that this parameterization of the dipolar coupling is generally applicable to pulsed DNP experiments with trityl OX063 in DNP juice, there must be something unusual about XiX and TOP DNP. An explanation that comes to mind is that also for TOP and XiX, a fanning out of the magnetization occurs after repeated cycles of polarization transfer. As this happens, trajectories will likely obtain larger x- and y-components, which means the scaling factor effectively increases and the transfer of polarization speeds up. In the case of TOP and XiX, where the calculated trajectories are rather confined [Figs. 7(a) and 7(b)], it is an advantageous effect.

Finally, the fanning out may also offer an explanation for the very good performance of XiX DNP at 7 MHz and, subsequently, flat nutation frequency dependence [Fig. 6(c) and Table S1]. Numerical simulations predict a 6-fold increase of the enhancement factor going from $\varepsilon_B = -19$ at 7 MHz to $\varepsilon_B = -121$ at 36 MHz [see Fig. 6(a)]. In addition, the theoretical scaling factor increases with the nutation frequency (Table S1). This means that at low nutation frequency, the fanning out is advantageous, leading to a higher effective scaling factor. However, at higher nutation frequencies, where the scaling factor of XiX is already large, it becomes detrimental. Like in TPPM, it leads to an increase in the optimal repetition time (Table S1) and a reduced gain in sensitivity.

Previously, in NOVEL experiments at X band, we investigated the dependence of the enhancement factor on the concentration of trityl OX063 in DNP juice.[17] The enhancement factor increased approximately linearly with the concentration up to 7–8 mM, where an abrupt deterioration of the enhancement as well as drastic changes in the echo-detected EPR spectrum were observed. In experiments at Q band, we also observe a general increase of the enhancement factors with the polarizing agent concentration, up to 7–8 mM. However, how much is gained at a higher concentration seems to depend on the sequence. In particular, we find that TOP DNP benefits more from a higher polarizing agent concentration than XiX. At the moment, we have no good explanation for this phenomenon, but increased interactions between the unpaired electrons of trityl likely play a role. At 6.4 mM, the average strength of the electron–electron dipolar coupling is 200 kHz, which is significant compared to the electron–proton dipolar coupling. This may cause interference effects that vary from sequence to sequence. Electron–electron interactions, in any case, reduce the phase memory time. Although not fully consistent with experimental observations [Fig. 8(b)], theory and numerical simulations indicate that the effect of fast transverse relaxation on the transfer of polarization depends on the sequence [compare Figs. 7(d) and 8(a)].

The gain in sensitivity one eventually obtains with pulsed DNP for a given average microwave power follows from a subtle interplay between the electron and nuclear relaxation rates and the properties of the sequence such as scaling factor, response to line-broadening, optimal repetition rate, and dependence on polarizing agent concentration. Some of these properties (scaling factor, response to line-broadening) are readily found from the analysis of a single cycle of polarization transfer. Others (optimal repetition rate, concentration dependence) require the modeling of many transfer cycles as well as the diffusion of the enhanced polarization into the sample. We did not pursue this here because spin dynamics simulations of large solid-state systems are still computationally very costly. This would make scanning large numbers of DNP conditions by means of numerical simulations cumbersome. Moreover, setting the parameters of such a complex spin system must be performed with care. Extensive testing against experiments will be necessary before larger models can be used effectively to design DNP pulse sequences. Our investigations, however, show that such simulations will add value.

VI. CONCLUSION

At 1.2 T, the new TPPM (two-pulse phase modulation) DNP pulse sequence efficiently polarizes bulk proton spins. It, however, requires a relatively high nutation frequency, i.e., 33 MHz, compared

to a proton Larmor frequency of 51 MHz. The XiX (X-inverse-X) DNP sequence is less efficient but already performs well at nutation frequencies as low as 7 MHz. The theoretical description of the transfer of polarization induced by TPPM, or any other periodic DNP pulse sequence, in a dipolar-coupled electron–nuclear spin system is under control. Numerical simulations of this process give an indication of the gain in sensitivity that can be generated for NMR of the bulk proton spins, but they do not account for all experimental observations. Augmented modeling will, therefore, be important for the design of new and improved DNP pulse sequences, for example, with the help of optimal control. Moreover, it will offer better guidance for the development of dedicated instruments, in particular suitable microwave sources, for pulsed DNP at high magnetic fields.

SUPPLEMENTARY MATERIAL

The supplementary material includes the EPR characterization of samples used for pulsed DNP experiments; simulated parameter scans of all TPPM DNP conditions of interest; supporting experimental data for Table I, namely, ^{1}H NMR spectra with and without DNP, measurements of the ^{1}H longitudinal relaxation time and build-up times of the bulk ^{1}H polarization; investigation of the DNP conditions close to resonance for XiX DNP; investigation of the dependence of the build-up time of bulk ^{1}Hs on the repetition time for TPPM DNP; supporting experimental data for the investigation of the nutation frequency dependence for XiX and TOP DNP; offset dependence of the mismatch for TPPM DNP; ^{1}H NMR spectra of the 2.1 mM trityl OX063 sample enhanced by XiX and TOP DNP; and the trajectory $\tilde{S}_z(t)$ in the modulating frame for BEAM at 0.34 T.

AUTHOR DECLARATIONS

Conflict of Interest

The authors have no conflicts to disclose.

Author Contributions

Venkata SubbaRao Redrouthu: Conceptualization (equal); Data curation (equal); Formal analysis (equal); Investigation (equal); Methodology (equal); Software (equal); Validation (equal); Visualization (equal); Writing – review & editing (equal). **Sanjay Vinod-Kumar**: Data curation (equal); Formal analysis (equal); Investigation (equal); Resources (equal); Validation (equal); Visualization (equal); Writing – review & editing (equal). **Guinevere**

04 April 2024 14:49:11

Mathies: Conceptualization (equal); Data curation (equal); Formal analysis (equal); Funding acquisition (lead); Investigation (equal); Methodology (equal); Project administration (lead); Resources (equal); Software (equal); Supervision (lead); Validation (equal); Visualization (equal); Writing – original draft (lead); Writing – review & editing (equal).

DATA AVAILABILITY

The data that support the findings of this study as well as the Matlab scripts that were used to analyze the DNP pulse sequences presented here are openly available in Zenodo at https://zenodo.org/record/8061361 and https://zenodo.org/record/8061384 . Scripts used for numerical simulations have been made available in the Spinach library at https://spindynamics.org.

REFERENCES

[1] T. Biedenbänder, V. Aladin, S. Saeidpour, and B. Corzilius, "Dynamic nuclear polarization for sensitivity enhancement in biomolecular solid-state NMR," Chem. Rev. **122**(10), 9738–9794 (2022).

[2] I. B. Moroz and M. Leskes, "Dynamic nuclear polarization solid-state NMR spectroscopy for materials research," Annu. Rev. Mater. Res. **52**(1), 25–55 (2022).

[3] C. D. Jeffries, "Dynamic orientation of nuclei by forbidden transitions in paramagnetic resonance," Phys. Rev. **117**(4), 1056–1069 (1960).

[4] C. F. Hwang and D. A. Hill, "New effect in dynamic polarization," Phys. Rev. Lett. **18**(4), 110–112 (1967).

[5] C. F. Hwang and D. A. Hill, "Phenomenological model for the new effect in dynamic polarization," Phys. Rev. Lett. **19**(18), 1011–1014 (1967).

[6] L. R. Becerra, G. J. Gerfen, R. J. Temkin, D. J. Singel, and R. G. Griffin, "Dynamic nuclear polarization with a cyclotron resonance maser at 5 T," Phys. Rev. Lett. **71**(21), 3561–3564 (1993).

[7] M. Rosay, L. Tometich, S. Pawsey, R. Bader, R. Schauwecker, M. Blank, P. M. Borchard, S. R. Cauffman, K. L. Felch, R. T. Weber, R. J. Temkin, R. G. Griffin, and W. E. Maas, "Solid-state dynamic nuclear polarization at 263 GHz: Spectrometer design and experimental results," Phys. Chem. Chem. Phys. **12**(22), 5850 (2010).

[8] M. Rosay, M. Blank, and F. Engelke, "Instrumentation for solid-state dynamic nuclear polarization with magic angle spinning NMR," J. Magn. Reson. **264**, 88–98 (2016).

[9] E. A. Nanni, A. B. Barnes, Y. Matsuki, P. P. Woskov, B. Corzilius, R. G. Griffin, and R. J. Temkin, "Microwave field distribution in a magic angle spinning dynamic nuclear polarization NMR probe," J. Magn. Reson. **210**(1), 16–23 (2011).

[10] A. Purea, C. Reiter, A. I. Dimitriadis, E. de Rijk, F. Aussenac, I. Sergeyev, M. Rosay, and F. Engelke, "Improved waveguide coupling for 1.3 mm MAS DNP probes at 263 GHz," J. Magn. Reson. **302**, 43–49 (2019).

[11] C. R. Donaldson, L. Zhang, M. Beardsley, M. Harris, P. G. Huggard, and W. He, "CNC machined helically corrugated interaction region for a THz gyrotron traveling wave amplifier," IEEE Trans. Terahertz Sci. Technol. **8**(1), 85–89 (2018).

[12] M. Cwiklinski, P. Bruckner, S. Leone, S. Krause, C. Friesicke, H. Massler, R. Quay, and O. Ambacher, in *2020 IEEE MTT-S International Microwave Symposium (IMS)* (IEEE, Los Angeles, CA, 2020), pp. 1117–1120.

[13] H. J. Kim, E. A. Nanni, M. A. Shapiro, J. R. Sirigiri, P. P. Woskov, and R. J. Temkin, "Amplification of picosecond pulses in a 140-GHz gyrotron-traveling wave tube," Phys. Rev. Lett. **105**(13), 135101 (2010).

[14] E. A. Nanni, S. M. Lewis, M. A. Shapiro, R. G. Griffin, and R. J. Temkin, "Photonic-band-gap traveling-wave gyrotron amplifier," Phys. Rev. Lett. **111**(23), 235101 (2013).

[15] A. Henstra, P. Dirksen, J. Schmidt, and W. T. Wenckebach, "Nuclear spin orientation via electron spin locking (NOVEL)," J. Magn. Reson. **77**(2), 389–393 (1988).

[16] T. V. Can, J. J. Walish, T. M. Swager, and R. G. Griffin, "Time domain DNP with the NOVEL sequence," J. Chem. Phys. **143**(5), 054201 (2015).

[17] G. Mathies, S. Jain, M. Reese, and R. G. Griffin, "Pulsed dynamic nuclear polarization with trityl radicals," J. Phys. Chem. Lett. **7**(1), 111–116 (2016).

[18] S. K. Jain, G. Mathies, and R. G. Griffin, "Off-resonance NOVEL," J. Chem. Phys. **147**(16), 164201 (2017).

[19] K. O. Tan, C. Yang, R. T. Weber, G. Mathies, and R. G. Griffin, "Time-optimized pulsed dynamic nuclear polarization," Sci. Adv. **5**(1), eaav6909 (2019).

[20] V. S. Redrouthu and G. Mathies, "Efficient pulsed dynamic nuclear polarization with the X-inverse-X sequence," J. Am. Chem. Soc. **144**(4), 1513–1516 (2022).

[21] N. Wili, A. B. Nielsen, L. A. Völker, L. Schreder, N. C. Nielsen, G. Jeschke, and K. O. Tan, "Designing broadband pulsed dynamic nuclear polarization sequences in static solids," Sci. Adv. **8**(28), eabq0536 (2022).

[22] A. E. Bennett, C. M. Rienstra, M. Auger, K. V. Lakshmi, and R. G. Griffin, "Heteronuclear decoupling in rotating solids," J. Chem. Phys. **103**(16), 6951–6958 (1995).

[23] I. Scholz, B. H. Meier, and M. Ernst, "Operator-based triple-mode Floquet theory in solid-state NMR," J. Chem. Phys. **127**(20), 204504 (2007).

[24] I. Scholz, J. D. van Beek, and M. Ernst, "Operator-based Floquet theory in solid-state NMR," Solid State Nucl. Magn. Reson. **37**(3–4), 39–59 (2010).

[25] R. Ramesh and M. S. Krishnan, "Effective Hamiltonians in Floquet theory of magic angle spinning using van Vleck transformation," J. Chem. Phys. **114**(14), 5967–5973 (2001).

[26] I. Scholz, P. Hodgkinson, B. H. Meier, and M. Ernst, "Understanding two-pulse phase-modulated decoupling in solid-state NMR," J. Chem. Phys. **130**(11), 114510 (2009).

[27] B. Blümich and H. W. Spiess, "Quaternions as a practical tool for the evaluation of composite rotations," J. Magn. Reson. **61**(2), 356–362 (1985).

[28] R. Shankar, M. Ernst, P. K. Madhu, T. Vosegaard, N. C. Nielsen, and A. B. Nielsen, "A general theoretical description of the influence of isotropic chemical shift in dipolar recoupling experiments for solid-state NMR," J. Chem. Phys. **146**(13), 134105 (2017).

[29] Previously, in Ref. 20, we incorrectly identified the Fourier coefficient $a_z^{(0,0)}$ of $U_{1S}^{-1}\rho(0)U_{1S}$ with $\rho(0) = -S_z$, as the alignment and swapped the DQ and ZQ terms in the expression for $\langle I_z \rangle(t)$.

[30] M. K. Bowman, C. Mailer, and H. J. Halpern, "The solution conformation of triarylmethyl radicals," J. Magn. Reson. **172**(2), 254–267 (2005).

[31] S. N. Trukhan, V. F. Yudanov, V. M. Tormyshev, O. Y. Rogozhnikova, D. V. Trukhin, M. K. Bowman, M. D. Krzyaniak, H. Chen, and O. N. Martyanov, "Hyperfine interactions of narrow-line trityl radical with solvent molecules," J. Magn. Reson. **233**, 29–36 (2013).

[32] G. T. Trammell, H. Zeldes, and R. Livingston, "Effect of environmental nuclei in electron spin resonance spectroscopy," Phys. Rev. **110**(3), 630–634 (1958).

[33] M. Bowman, L. Kevan, and R. N. Schwartz, "Analysis of matrix nuclei spin flip satellite lines in EPR spectra: Application to trapped hydrogen atoms," Chem. Phys. Lett. **30**(2), 208–211 (1975).

[34] H. J. Hogben, M. Krzystyniak, G. T. P. Charnock, P. J. Hore, and I. Kuprov, "*Spinach*—A software library for simulation of spin dynamics in large spin systems," J. Magn. Reson. **208**(2), 179–194 (2011).

[35] G. Bodenhausen, R. Freeman, and D. L. Turner, "Suppression of artifacts in two-dimensional *J* spectroscopy," J. Magn. Reson. **27**(3), 511–514 (1977).

[36] I. Marin-Montesinos, J. C. Paniagua, M. Vilaseca, A. Urtizberea, F. Luis, M. Feliz, F. Lin, S. Van Doorslaer, and M. Pons, "Self-assembled trityl radical capsules–implications for dynamic nuclear polarization," Phys. Chem. Chem. Phys. **17**(8), 5785–5794 (2015).

[37] In Ref. 19 as well as in Ref. 20, the terms $1 - e^{-rd_{on}/T_{BU}}$ and $1 - e^{-rd_{off}/T_{In}}$ were inadvertently placed above and below the fraction bar, respectively. Equation (17) is the correct expression.

[38] B. Corzilius, L. B. Andreas, A. A. Smith, Q. Z. Ni, and R. G. Griffin, "Paramagnet induced signal quenching in MAS–DNP experiments in frozen homogeneous solutions," J. Magn. Reson. **240**, 113–123 (2014).

04 April 2024 14:49:11

[39] M. Chávez and M. Ernst, "A continuous approach to Floquet theory for pulse-sequence optimization in solid-state NMR," J. Chem. Phys. **157**(18), 184103 (2022).

[40] B. Corzilius, A. A. Smith, and R. G. Griffin, "Solid effect in magic angle spinning dynamic nuclear polarization," J. Chem. Phys. **137**(5), 054201 (2012).

[41] M. H. Levitt and R. Freeman, "NMR population inversion using a composite pulse," J. Magn. Reson. **33**(2), 473–476 (1979).

[42] B. M. Fung, A. K. Khitrin, and K. Ermolaev, "An improved broadband decoupling sequence for liquid crystals and solids," J. Magn. Reson. **142**(1), 97–101 (2000).

04 April 2024 14:49:11